



High surface area mesoporous nanocast LaMO₃ (M = Mn, Fe) perovskites for efficient catalytic ozonation and an insight into probable catalytic mechanism

Shahzad Afzal, Xie Quan*, Jianlin Zhang

Key Laboratory of Industrial Ecology and Environmental Engineering (Ministry of Education), School of Environmental Science and Technology, Dalian University of Technology, Linggong Road 2#, Dalian 116024, PR China

ARTICLE INFO

Article history:

Received 31 October 2016

Received in revised form 19 January 2017

Accepted 25 January 2017

Available online 26 January 2017

Keywords:

Catalytic ozonation

Perovskite

Nanocasting

High surface area

Mesoporous

ABSTRACT

Mesoporous nanocast perovskites (NC-LaMnO₃ and NC-LaFeO₃) were synthesized by nanocasting technique using SBA-15 as a template and for the first time they were used in catalytic ozonation of 2-chlorophenol. For the purpose of comparison, uncast counterpart perovskites (CA-LaMnO₃ and CA-LaFeO₃) as well as Mn₃O₄ and Fe₂O₃ were also prepared by conventional citric acid assisted route. Nanocast perovskites possessed high specific surface area and large pore dimensions than uncast perovskites. Catalytic activity in terms of TOC removal followed the order of NC-LaMnO₃ > NC-LaFeO₃ > CA-LaMnO₃ > CA-LaFeO₃ > Mn₃O₄ > Fe₂O₃ > O₃ with 80, 68, 50, 43, 39, 33% and 25% respectively. A detailed study is conducted to discuss the mechanism of catalytic ozonation of selected NC-LaMnO₃ perovskite by using organic and inorganic hydroxyl radical's quenchers, FTIR, fluorescence spectroscopy, EPR, ATR-FTIR, XPS, LSV, H₂O₂ detection, Raman spectroscopy, TPR-H₂, R_{ct} value calculation, ozone utilization efficiency and ozone decomposition. It was found that hydroxyl radicals rather than surface peroxide, surface atomic oxygen, superoxide and singlet oxygen were the reactive oxygen species contributed to high catalytic activity. Moreover, high surface area as well as open porous structure of nanocast perovskites were believed to enhance the catalytic activity by surface reaction and easy access of reactants to the active sites.

© 2017 Elsevier B.V. All rights reserved.

1. Introduction

Heterogeneous catalytic ozonation is receiving an enormous attention in drinking as well as waste water treatment owing to its ability to enhance the degradation and mineralization of organic pollutants [1,2]. Various kinds of heterogeneous ozonation catalysts such as various metal oxides, metals/metal oxides loaded on supports and carbon materials etc have been used for water treatment with promising results. Carbon materials have high adsorption ability but can be oxidized during ozonation. Moreover, due to steric hindrance, supported metals or metal oxides based catalysts experienced some problems such as distorted textural properties (decrease in specific surface area, pore size and pore volume), an uneven active components distribution, pore blockage and poorly accessible active sites. Furthermore, due to some complex procedures for the synthesis of porous materials

and complexity of active components in supported metals/metal oxides catalysts, investigation of catalytic ozonation mechanism is still a dilemma [1,3,4]. The key to a practical application of catalytic ozonation is to find/synthesize an effective catalyst. So there is always a quest to fabricate or find a solid catalyst with high activity as well as stability. Perovskite like mixed metal oxides possess well-defined and crystalline structure with general unit formula of ABO₃, whereas A is cation from alkaline earth or alkali metal group and rare-earth group while B represents a transition metal from the groups 3d, 4d and 5d [5]. Perovskite-like mixed metal oxides have been applied as cheap alternative materials for noble metals-based catalysis such as electrocatalysis [6], oxidation of VOCs and NO_x removal [7,8]. Perovskite type structures have some unique characteristics compared to other common mixed-metal oxides. They can be substituted at A and/or B sites which can create defects structure or/and can alter the oxidation state of A and/or site B. The catalytic activity of the perovskite depends on oxidation states of the transition metals, the quantity of non-stoichiometric oxygen and the presence of defects structure. The oxygen vacancies are favorable

* Corresponding author.

E-mail address: quanxie@dlut.edu.cn (X. Quan).

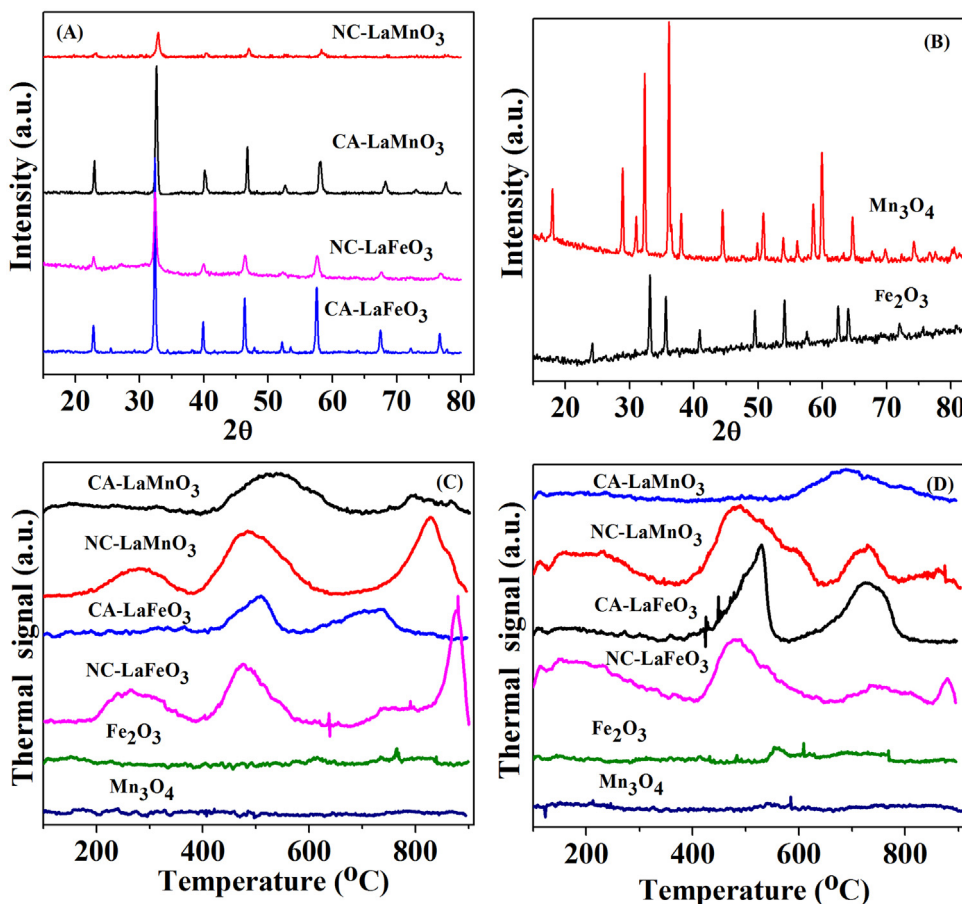


Fig. 1. Wide-angle XRD patterns of (A) perovskites and (B) Metals Oxides, (C) TPD-NH₃ and (D) TPD-CO₂ of all catalysts.

for the oxidation because they can enhance the mobility of lattice oxygen [9].

The textural properties and phase purity of perovskites depends upon the preparation methods. Several synthesis methods such as sol-gel [10], micro-emulsion [11], coprecipitation [12], freeze-drying [13], flame-hydrolysis [14] and citrate complexation [15] are used to prepare perovskites. Except citrate complexation method, all the aforementioned methods require enormous quantity of organic solvents, expensive reagents and complex multi-step preparation procedures. Unfortunately, in citrate method, the high-temperature treatment generally resulted to low specific surface area of perovskites. Nanocasting is an effective technique for the synthesis of various nonsiliceous mesoporous materials with high surface area which have been used for catalysis, energy storage and sensing etc [16–18].

In the past, few studies were carried out to investigate the catalytic activity of perovskites in ozonation [19–22]. In all those studies, La-containing perovskites synthesized by the conventional citrate method were used. To the best our knowledge, there is no report to use high surface area nanocast perovskites in catalytic ozonation. Manganese and iron are cheap, environment friendly and naturally abundant transition metals. Furthermore, both the metals exist in multi-valence state which undergoes redox couple during catalytic ozonation. Due to these properties both are extensively used in catalytic ozonation. Here, in our research work, nanocast mesoporous perovskites NC-LaMnO₃ and NC-LaFeO₃ are synthesized by using ordered mesoporous SBA-15 as a hard template. Based on the investigations of previous researchers, it is evidenced that the mechanistic study of catalytic ozonation is complex, unclear and controversial. Using perovskites in catalytic

ozonation is still not very popular and no detailed study on the mechanism of their catalytic activity is available.

The previously published research works regarding the use of perovskites mainly dealt with the kinetics and comparative catalytic activities of different perovskites. Moreover those studies did not investigate different aspects of catalytic activity such as surface area dependent activity, catalysts prepared by different methods (conventional citric acid assisted route and nanocasting), comparative catalytic activity with counterpart metal oxides prepared by same method, detailed mechanism of catalytic ozonation based on advanced surface characterization such as probing acidic and basic active sites, role of redox couple and nature of reactive oxygen species. So the purpose of this research work is to investigate the above mentioned aspects. Moreover, as our manuscript dealt with the use of high surface area nanocast perovskites for catalytic ozonation. There are some advantages of such structures in catalytic ozonation. For improving the catalytic activity, large surface area, the effective utilization of surface area, fast mass transport and enhanced exposure of active components at the solid-liquid interface play an important role [23,24]. In some catalysts, it is not easy for the reactants to reach the internal structures (active sites) due to steric effect which limits their applications. In such situation, a large number of active components/sites are condensed in the bulk of catalyst which minimizes the direct exposure of reactants which ultimately decline the catalytic activity. So it is highly desirable to use catalysts with large effective surface area and enhanced accessibility. Herein, 2-chlorophenol (2-CP) is chosen as a target for degradation/mineralization as it is one of the top priority pollutants [25]. A detailed study is conducted to discuss the mechanism of catalytic ozonation of nanocast perovskite by using organic and

Table 1

Textural properties, crystal sizes and cell parameters of all catalysts.

| Sample | BET Surface Area (m ² g ⁻¹) | Pore diameter (nm) | Pore Volume (cm ³ g ⁻¹) | Crystal Size (nm) | Cell Parameters (nm) | | |
|--------------------------------|---|--------------------|---|-------------------|----------------------|--------|--------|
| | | | | | a | b | c |
| SBA-15 | 710.90 | 9.45 | 0.80 | — | — | — | — |
| CA-LaMnO ₃ | 15.0 | 3.08 | 0.06 | 24.16 | 0.3880 | 0.3880 | 0.3880 |
| CA-LaFeO ₃ | 8.89 | 3.06 | 0.03 | 28.61 | 0.3926 | 0.3926 | 0.3926 |
| NC-LaMnO ₃ | 119.60 | 7.70 | 0.33 | 17.58 | 0.3880 | 0.3880 | 0.3880 |
| NC-LaFeO ₃ | 92.25 | 4.90 | 0.33 | 19.82 | 0.3926 | 0.3926 | 0.3926 |
| Mn ₃ O ₄ | 10.37 | 3.43 | 0.043 | 29.90 | 0.5765 | 0.5765 | 0.9442 |
| Fe ₂ O ₃ | 7.00 | 3.50 | 0.023 | 30.38 | 0.5424 | 0.5424 | 0.5424 |

inorganic hydroxyl radical's quenchers, fluorescence spectroscopy, EPR, ATR-FTIR, Raman spectroscopy, XPS measurement, LSV, H₂O₂ detection, FTIR, TPR-H₂, R_{ct} value calculation, ozone utilization efficiency and ozone decomposition.

2. Materials and methods

2.1. Preparation of catalysts, their characterizations, catalytic ozonation and analytical procedures

Nanocast perovskites were synthesized by the procedure developed by Nair et al. [26]. The as-purchased SBA-15 was used as a template for the preparation of mesoporous LaMnO₃ and LaFeO₃. Typically, 1.0 g SBA-15 was stirred in 10 mL deionized water for 20 min to make a suspension. For each perovskite preparation, 3.0 mmol each of La(NO₃)₃·6H₂O, Mn(NO₃)₂ or Fe(NO₃)₃·9H₂O were added to citric acid dissolved in 10 mL ethanol to get an equimolar solution. The molar ratio of citric acid to total metal ions was selected to be 1:2 (1:1+1). This solution was added drop wise to SBA-15 suspension and stirred for 8 h at room temperature. In order to get the powder, the solvent was evaporated/dried at 80 °C for 24 h, ground well and ultimately calcined at 500 °C for 5 h (5 °C min⁻¹) in air to remove the organic constituent. For higher loading, impregnation was repeated with half of the amount of the aforementioned precursors (citric acid and metal nitrates) and calcined at 700 °C for 8 h (5 °C min⁻¹). Finally, the silica template was removed by stirring it 3–4 times in 2 M NaOH aqueous solution at room temperature. Ultimately, the product was washed with water and ethanol repeatedly until it became neutral (approximately pH 7) and dried overnight at 80 °C. Mn and Fe based catalysts obtained by nanocasting method are represented as NC-LaMnO₃ and NC-LaFeO₃. For comparison, the same perovskites were prepared in one step at calcination temperature of 700 °C by following the above mentioned protocol with citric acid assistance but without adding any template. Citric acid assisted perovskites are represented as CA-LaMnO₃ and CA-LaFeO₃. Furthermore, manganese oxide (Mn₃O₄) and iron oxide (Fe₂O₃) were synthesized by the same citric acid assisted method and their catalytic activity was compared to that of perovskites.

A detail about XRD, TEM, N₂ sorption isotherms, Pyridine FTIR, pH_{pzc}, FTIR, EPR, ICP-AES, TGA, ATR-FTIR analyses, XPS, LSV, Raman Spectroscopy, TPR-H₂ and TPD-NH₃ and TPD-CO₂ are given in the supplementary information S1. Detailed procedures regarding catalytic ozonation and various analyses are provided in supplementary information S2.

3. Results and discussion

3.1. Characterizations of catalysts

The XRD patterns of perovskites prepared by conventional citrate or nanocasting methods exhibited the single-phase crystalline perovskite structure with no additional peaks/phases of La, Fe,

Mn or their oxides (Fig. 1A). All the peaks are designated to the perovskites crystalline phases of CA-LaFeO₃ and NC-LaFeO₃ (PDF#75-0541) and CA-LaMnO₃ and NC-LaMnO₃ (PDF#75-0440). CA-LaMnO₃ and CA-LaFeO₃ showed highly crystalline structures as evidenced from the well-resolved and high intensity peaks. NC-LaMnO₃ and NC-LaFeO₃ exhibited low-intensity broad peaks indicating their small particles size. XRD of manganese oxide and iron oxide prepared by citric acid assisted route showed hausmanite Mn₃O₄ (PDF#80-0382) and Fe₂O₃ (PDF#73-2234) according to the standard JCPDS (Fig. 1B). Moreover, we calculated the crystal sizes by applying Scherrer equation and analyzed the cell parameters from the XRD patterns by MDI Jade 6.0 software to confirm the structure of these materials. The data regarding crystal sizes and cell parameters are given in Table 1.

The N₂ sorption isotherms of NC-LaMnO₃ and NC-LaFeO₃ showed type IV character with a well-developed and distinct hysteresis loop in the relative pressure (P/P₀) range of 0.45–1.0, suggesting the mesoporous characteristics of materials (Fig. S1A). It is observed in Table 1 and Fig. S1B, the specific surface area, pore diameter and pore volume of the nanocast perovskites were significantly higher than the uncast perovskites and metal oxides. These improved textural characteristics of nanocast perovskites are due to the templating effect of mesoporous SBA-15 during the synthesis of perovskites.

TEM observations of CA-LaMnO₃ and CA-LaFeO₃ showed a highly disordered and aggregated structure (Fig. 2A, B). But NC-LaMnO₃ and NC-LaFeO₃ showed some ordered domains as well as a fraction of less defined and worm-like disordered regions (Fig. 2C, D). The presence of these disordered regions is due to the incomplete filling of the precursors in the mesopore volume of SBA-15. In fact, after removing the template, the mesoporous ordered framework SBA-15 is destroyed, giving rise to a disordered structure. Although the materials seemed to be disordered, but still had quite open and accessible porous structure, capable of facilitating the access of the reactants to catalytically active sites which subsequently can improve the catalytic activity. HRTEM clearly indicated lattice fringes have distance of 0.285 nm and 0.238 nm which are nearly same to (110) and (111) lattice planes in XRD respectively. SEM images of metal oxides (Fe₂O₃ and Mn₃O₄) are provided in Fig. S2. Both the images showed an irregular and distorted morphology with no exact shape to accurately measure particle sizes. However, the average particle sizes of Mn₃O₄ and Fe₂O₃ were about 39.68 μm and 35.24 μm respectively.

Furthermore, TPD-NH₃ and TPD-CO₂ experiments were carried out to characterize acidic and basic sites respectively (Fig. 1C and D). TPD-NH₃ and TPD-CO₂ results showed that the perovskites surface is heterogeneous showing different sites of various strengths for CO₂ and NH₃ adsorption. The intensity of peaks for NC-LaMnO₃ and NC-LaFeO₃ was stronger than the CA-LaMnO₃, CA-LaFeO₃, Fe₂O₃ and Mn₃O₄. Moreover, Mn₃O₄ and Fe₂O₃ did not show any obvious and distinct NH₃ and CO₂ desorption peaks for acidic and basic sites respectively. Nanocast perovskites showed high concentration of acidic and basic Lewis surface sites as compared to uncast

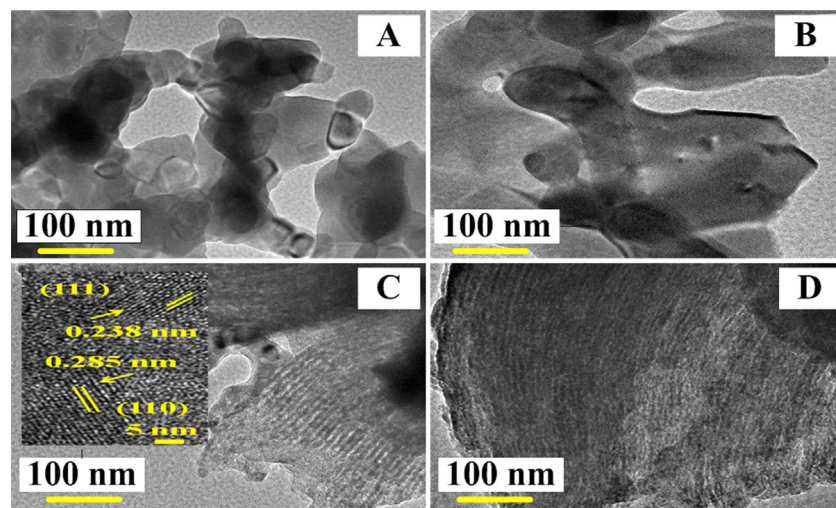


Fig. 2. TEM of (A) CA-LaMnO₃, (B) CA-LaFeO₃, (C) NC-LaMnO₃ and (D) NC-LaFeO₃. The inset in Fig C is the HRTM of NC-LaMnO₃.

perovskites and metal oxides. The peaks shown at comparatively lower temperatures are attributed to weak acidic and basic sites while at high temperatures are assigned to strong acidic and basic sites. The high acidity and basicity in nanocast perovskites maybe be originated from large amount of acidic and basic sites due to high surface area [27]. Similarly to get more insight, the nature of Lewis and Brønsted acid sites of selected NC-LaMnO₃ were probed by pyridine adsorption combined with FTIR. As shown in Fig. S3, NC-LaMnO₃ exhibited obvious IR bands at around 1444, 1490, 1545 and 1603 cm⁻¹ which are attributed to pyridine adsorbed onto Lewis acid, both Lewis + Brønsted acid, strong Brønsted acid and Lewis acid sites respectively. Some extra peaks are also shown which may be ascribed to some free pyridine [28,29].

3.2. Removal of TOC and degradation of 2-chlorophenol in different processes

As catalytic ozonation is more efficient than single ozonation for the removal of TOC, so at first, the TOC removal was investigated. As shown in Fig. 3A, 25.0% TOC was removed after 75 min in ozonation alone. However in catalytic ozonation, TOC removal increased in the order of NC-LaMnO₃ > NC-LaFeO₃ > Ca-LaMnO₃ > CA-LaFeO₃ > Mn₃O₄ > Fe₂O₃ with 80, 68, 50, 43, 39, and 33% respectively. NC-LaMnO₃ and NC-LaFeO₃ with high surface areas showed the best performance than CA-LaMnO₃ and CA-LaFeO₃ with low surface areas. Similarly, the catalytic activity of Mn₃O₄ and Fe₂O₃ synthesized by citrate assisted method was lower than all kinds of perovskites. Mn-based catalysts were more effective than the Fe-based catalysts. It is evidenced that high surface area and wide pore dimensions played an important role in enhancing the catalytic activity by effectively exposing more reactive sites and reducing the impedance for the reactants to reach the active sites. Similarly NC-LaMnO₃ showed the strongest peaks in TPD-NH₃ and TPD-CO₂ experiments for acidic and basic sites. Mn₃O₄ and Fe₂O₃ did not show any obvious peaks for these sites but citric acid assisted perovskites has obvious peaks as compared to these metal oxides.

Furthermore, one of the best catalysts (NC-LaMnO₃) was selected and investigated its comparative effectiveness in the degradation of 2-CP to ozonation alone. Similarly, NC-LaMnO₃ would be used to discuss in detail the mechanism of catalytic ozonation. As shown in Fig. S5A, 100 and 91% 2-CP were degraded at 45 and 75 min in catalytic ozonation and sole ozonation respectively. Adsorption on NC-LaMnO₃ resulted in 9.0% removal of 2-CP which

was too small to make a significant contribution to the removal of 2-CP, so it could be ignored when compared to the ozonation and catalytic ozonation. NC-LaMnO₃ showed a minimal influence on the degradation of 2-CP. The insignificant catalytic degradation of 2-CP could be corresponded to the competition between 2-CP and its degraded intermediates products for reactive oxygen species and active sites. So it is suggested that 2-CP was predominantly removed by ozone in solution while reactive oxygen species effectively mineralized the organic intermediates. Furthermore, the rate of TOC removal was much lower than the degradation, suggesting that during the degradation of 2-CP, some organic intermediates were produced, which were reluctant to further mineralization.

In accordance to the degradation pattern/TOC removal, the pH of solution decreased from initial pH of 5.56 to 3.40 and 5.18 in ozonation and catalytic ozonation respectively, which suggested the formation of acidic intermediates during degradation (Supplementary information: Fig. S5B). The final pH in ozonation alone was lower than catalytic ozonation, indicating the accumulation of acidic intermediates in solution that could not be mineralized further, leading to lower TOC removal. Differently, the final pH of solution was larger in catalytic ozonation than ozonation alone, probably due to the production of reactive oxidative species which could mineralize the acidic intermediates effectively. It should be noted that before conducting the catalytic ozonation experiments, the effect of nanocast catalysts on solution pH was investigated, showing no/negligible effect (approximately 0.10 unit rise) as they were washed multiple times with deionized water until neutrality.

3.3. Stability of the catalyst

For testing the stability of the NC-LaMnO₃ after catalytic reaction, the catalyst was recycled (by sedimentation and centrifugation) and washed multiple times with deionized water. It was found that the TOC removal was slightly decreased from 80 to 70% in the first recycling run, while in the second and third run, the TOC removal was nearly stable (Fig. S6A). 0.10 mg L⁻¹ Mn leaching was detected which might be responsible to decrease the catalytic activity. To investigate the role of leached Mn in catalytic activity, the suspension was filtered and its ozonation with the same initial concentration of TOC was carried out without catalyst. However, the leached Mn did not show any obvious (negligible effect) catalytic activity (data not shown). Furthermore, after ozonation, the structural and textural stability were investigated by XRD and BET measurements. Here the XRD, BET surface area and pore

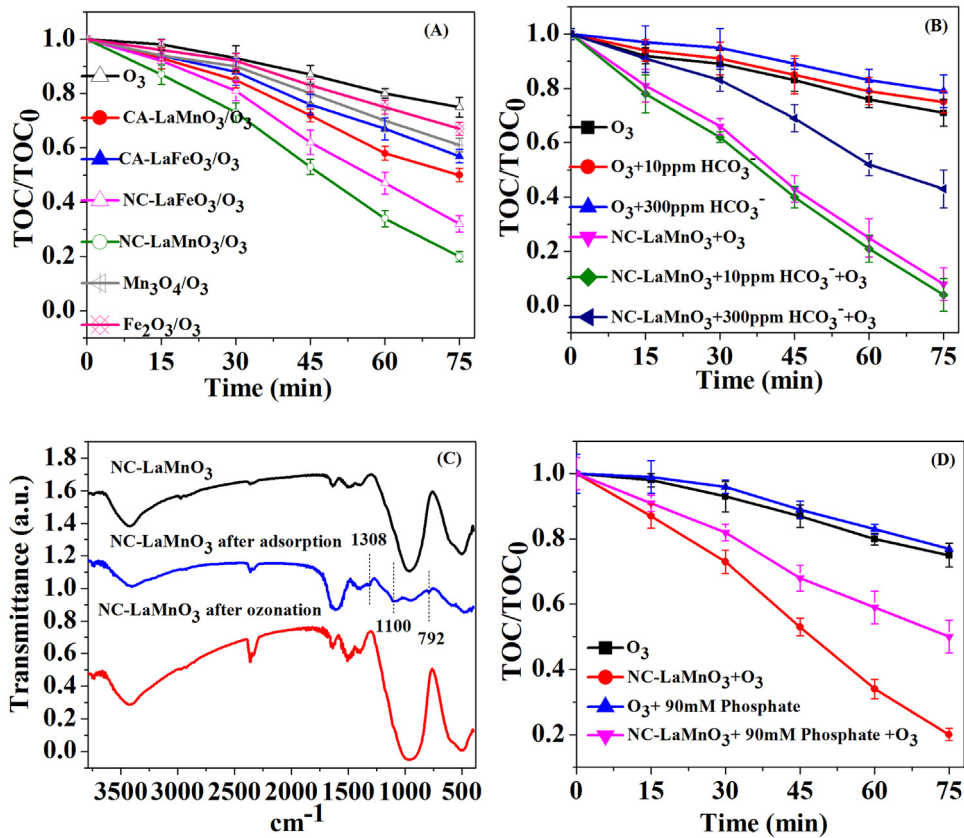


Fig. 3. (A) Comparison of TOC removal, (B) effect of bicarbonate on catalytic activity (C), FTIR spectra of NC-LaMnO₃ before ozonation, after adsorption of organic intermediates and after ozonation and (D) effect of phosphate on catalytic activity. Experimental conditions: Gaseous [O₃] = 20 mg L⁻¹; O₃ flow rate = 4 mg min⁻¹, volume of 2-CP solution = 1 L, Catalyst dose (if used) = 0.30 g L⁻¹, [2-CP] = 50 mg L⁻¹, initial pH = 5.56, Temperature = 25 °C.

dimensions are important as the nanocasting catalyst showed weak crystallinity and high surface area. It was found that there were no significant differences in the crystallinity and textural properties of the catalyst (Fig. S6B–D). So it is deduced that NC-LaMnO₃ has high catalytic activity as well as good stability.

4. Discussion on catalytic ozonation mechanism

4.1. Use of organic and inorganic scavengers

The use of 150 ppm *tert*-butanol (TBA) as a •OH scavenger showed no significant effect to decline the degradation of 2-CP (Fig. S5A), suggesting that it was mainly degraded by sole ozonation while •OH mainly mineralized the organic intermediates. Unfortunately, the use of TBA can increase the TOC value of the solution, so it is not appropriate to use TBA in such kind of experiments. In drinking and waste water, the presence of carbonate and bicarbonate also compete for •OH. Carbonate and bicarbonate are stronger radical scavengers due to their higher reaction rate constant with •OH [30]. These ions react with OH to produce carbonate radical (Eqs. (1)–(2)).

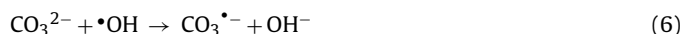


$$K_{\cdot\text{OH}} = 8.5 \times 10^6 \text{ M}^{-1} \text{ s}^{-1}$$



$$K_{\cdot\text{OH}} = 3.9 \times 10^8 \text{ M}^{-1} \text{ s}^{-1}$$

At the neutral pH condition, the inorganic carbon in water is mainly in the form of bicarbonate. So in order to increase the concentration of bicarbonate, the pH of reaction medium was adjusted to 9.0. In water, the concentration of bicarbonate is significantly higher than that of organic pollutants, so the bicarbonate can be the main scavenger of •OH [30]. As shown in Fig. 3B, 10 and 300 ppm HCO₃⁻ slightly inhibited TOC removal in ozonation alone. But in catalytic ozonation, 10 ppm HCO₃⁻ slightly enhanced TOC removal. This phenomenon is attributed to the production of H₂O₂ and its consumption by HCO₃⁻ and other species which produce •OH during catalytic ozonation as shown in the following equations [31,32].



In above equations, bicarbonate accelerated the initiation of •OH. This situation is attributed to the fact that HCO₃⁻ acted as a promoter to decompose O₃ in the presence of H₂O₂ [33]. On contrary, increasing concentration of HCO₃⁻ to 300 ppm strongly inhibited the catalytic activity. This means that bicarbonate scavenged •OH, which ultimately inhibited the overall mineralization process. So the inhibiting effect of the bicarbonate confirmed that the mineralization proceeded via the generation of •OH in the reaction medium [32]. The inhibiting effect of bicarbonate on removal of TOC was larger in catalytic ozonation than that in single ozonation.

4.2. Effect of changing initial pH on catalytic ozonation

In heterogeneous catalytic ozonation, pH of the reaction medium can affect the surface properties of the catalyst, ozone decomposition into reactive oxygen species and charge of ionic organic molecules. The pH_{pzc} of NC-LaMnO₃ is 8.98 (Fig. S7B), so the catalyst surface can be neutral, protonated or deprotonated at pH equal, far below or far above 8.98. With increasing initial solution pH from 3.0 to 9.0, TOC removal increased but at pH 11, it was insignificantly decreased (Fig. S7A). The catalytic activity was highest at pH 9.0~ pH_{pzc} (neutral charged surface) but insignificantly decreased at pH 3.0 ($pH < pH_{pzc}$ or protonated surface) and pH 11.0 ($pH > pH_{pzc}$ or deprotonated surface). These observations suggest that the catalyst could work at a wide range of pH. Neutral charged surface (Mn-OH) and protonated surface (Mn-OH⁺) showed comparatively high catalytic activity than deprotonated surface (Mn-O⁻). With respect to ozone interaction with catalyst surface, protonated surface OH⁺ is a weaker nucleophile than the O of neutral charged surface OH and deprotonated surface hydroxyl groups cannot offer the electrophilic H to ozone. Therefore, protonated and deprotonated surfaces minimized the binding of O₃ to surface hydroxyl groups which decreased the catalytic activity. Under our actual experimental conditions ($pH 5.56 < pH_{pzc}$), protonated surface (MnOH₂⁺) is also catalytically active, suggesting that O₃ due to its resonance structures (electrophilic and nucleophilic nature) could also interact with Bronsted acid –OH₂⁺ of the MnOH₂⁺ via electrostatic forces or/and hydrogen bonding to produce •OH. With respect to organic intermediates adsorption, protonated surface could facilitate the adsorption of organic acids by electrostatic attraction, while deprotonated surface could not favor adsorption of organics due to weaker electrostatic attraction. At pH 11.0, TOC removal decreased which was due to the fact that the mineralization of organic acids might be decreased in the bulk solution as well as on the surface of the catalyst [28]. These results showed that organic intermediates mineralization occurred on the surface of the catalyst as well as in the solution.

4.3. Ozone dynamics in terms of O₃ utilization efficiency (R_u %), R_{ct} value calculation and ozone decomposition

The effect of the catalyst on ozone decomposition and generation of •OH was explored. In order to understand the mass balance of ozone in gas and liquid phase, the concentrations of ozone in the influent (applied gas) and effluent gas (off gas) were monitored. The mass balance of ozone can be expressed as follow [34].

$$[O_3]_I = [O_3]_0 + [O_3]_R + [O_3]_C \quad (9)$$

Where [O₃]_I, [O₃]₀, [O₃]_R and [O₃]_C represent the concentrations of total applied inlet ozone, off gas, residual and consumed ozone respectively. [O₃]_C can be calculated as

$$[O_3]_C = [O_3]_I - ([O_3]_0 + [O_3]_R) \quad (10)$$

So based on the above parameters and the mass balance principle, the ozone utilization efficiency (R_u%) can be calculated by Eq. (11).

$$R_u\% = \frac{\int_0^t F([O_3]_I - [O_3]_0) dt - V[O_3]_R}{\int_0^t F[O_3]_I dt} \times 100 \quad (11)$$

Whereas F is the flow rate of gas and V is volume of solution. For the practical application of catalytic ozonation, the production cost of ozone is always considered. So a catalyst with high ozone utilization efficiency can decrease the cost of ozone. As shown in Fig. S7C, [O₃]_R reached to maximum of 0.52 mg L⁻¹ at 15 min, and then declined to 0.28 mg L⁻¹ at 75 min in catalytic ozonation. On other hand, [O₃]_R

in ozonation alone was increasing with time and reached to maximum of 1.30 mg L⁻¹ at 75 min. It can also be noted that at each interval of time, the residual ozone in case of NC-LaMnO₃ was lower than ozonation alone. Similarly at each instant of time, [O₃]₀ was higher in ozonation alone than catalytic ozonation. These observations indicated that more ozone was consumed immediately in the presence of NC-LaMnO₃ than ozonation alone. As shown in Fig. S8, ozone utilization with NC-LaMnO₃ was promoted than with ozonation alone. At each instant of time, R_u% in case of catalytic ozonation was higher than ozonation alone. As in our study, catalytic ozonation aimed to mineralize 2-CP, so the amount of ozone consumed per unit mass of TOC removed can be calculated by Eq. (12) [1].

$$\eta = \frac{R_u \int_0^t F[O_3]_I dt}{V([TOC_0] - [TOC_t])} \quad (12)$$

The quantity of ozone consumed per unit mass of TOC showed an opposite trend as compared to ozone utilization. At each interval of time, η was lower in catalytic ozonation than single ozonation (Fig. S8). It meant that NC-LaMnO₃/O₃ process efficiently used ozone than the single ozonation. In other words, ozone could be efficiently decomposed into reactive species which ultimately mineralize 2-CP at the expense of lower amount of ozone.

It is difficult to quantify the generated •OH directly but the evolution of •OH in the presence of catalysts can be compared. For this, Elovitz and Von Gunten proposed the R_{ct} concept, which is the ratio of the exposure of the •OH and ozone concentration at any given time in the reaction [35].

$$R_{ct} = \frac{\int_0^t [\cdot OH] dt}{\int_0^t [O_3] dt} \quad (13)$$

This is an experimental procedure to test the concentrations of the transient •OH and ozone. It represents the transformation efficiency of ozone into •OH. For R_{ct} value calculation, p-CBA is usually taken as a model pollutant for degradation. The R_{ct} value can be calculated by plotting p-CBA degradation as a function of ozone exposure.

$$\ln \frac{[p-CBA]_t}{[p-CBA]_0} = -k_{\cdot OH/p-CBA} R_{ct} \int_0^t [O_3] dt \quad (14)$$

From Eq. (14) and the slope of the curves in Fig. S9, the R_{ct} values of ozonation alone and catalytic ozonation were calculated to be 3.74×10^{-7} and 1.41×10^{-6} . So based on the R_{ct} values, it can be deduced that catalytic ozonation generated more •OH than ozonation alone, which is in agreement with the mineralization efficiency. It can be concluded that NC-LaMnO₃ exhibited high catalytic activity owing to its high R_{ct} value than ozonation alone.

In our study, it is hypothesized that the interaction of O₃ with the surface of catalyst and its decomposition into reactive species is considered to be a key factor for catalytic activity. To investigate this interaction, in a batch type reactor without 2-CP, aqueous O₃ decomposition in the presence and absence the NC-LaMnO₃ and NC-LaFeO₃ was studied (Supporting information S2). As compared to ozonation alone, O₃ decomposition in the presence of catalysts was obviously enhanced (Fig. S10). As compared to catalytic process, the concentrations of ozone were higher at each instant during ozonation alone, suggesting that the presence of the catalysts was beneficial for the decomposition of O₃, which might play a crucial role in the catalytic ozonation. Decomposition of O₃ in ozonation and catalytic ozonation obeyed first-order kinetics which can be expressed as

$$-d[O_3]/dt = K_{obs}[O_3] \quad (15)$$

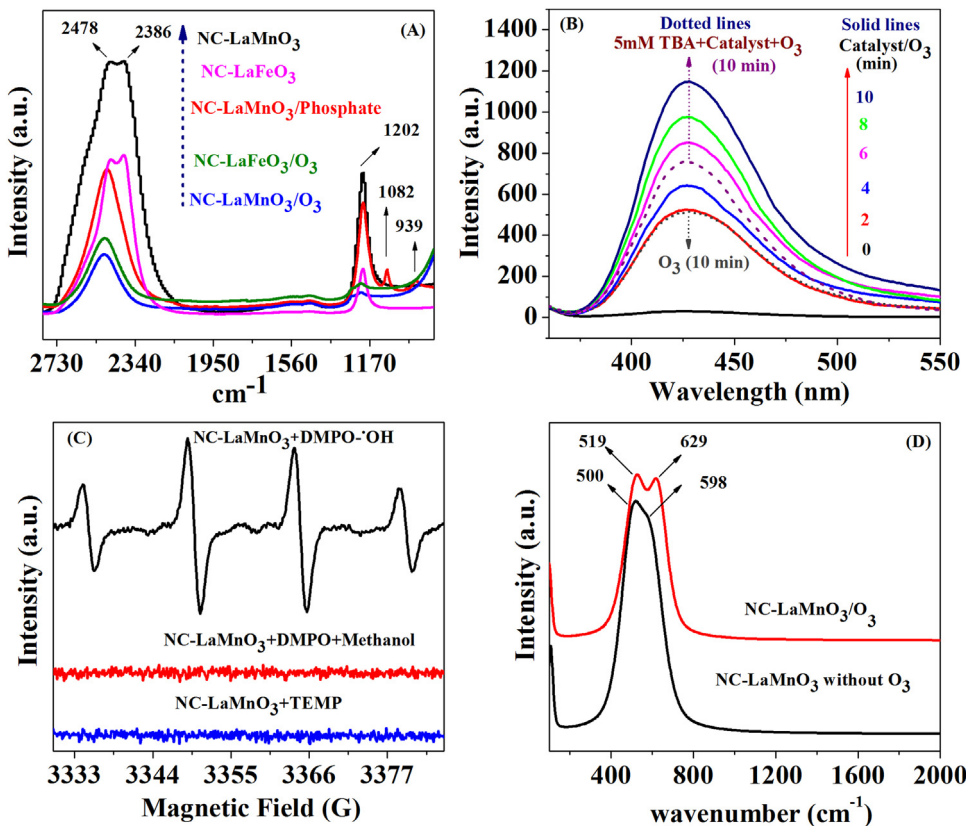


Fig. 4. (A) ATR-FTIR of NC-LaMnO₃/D₂O interface in the presence and absence of phosphate and ozone saturated solution while NC-LaFeO₃/D₂O interface in the presence and absence of ozone saturated solution, (B) Fluorescence spectra at different reaction times in ozonation, catalytic ozonation and in the presence of TBA, (C) EPR for NC-LaMnO₃ in the presence of ozone and (D) Raman spectra of NC-LaMnO₃ in the presence and absence of ozone. Experimental conditions for B: Gaseous [O₃] = 20 mg L⁻¹; O₃ flow rate = 4 mg min⁻¹, Catalyst doze (if used) = 0.30 g L⁻¹, initial pH = 5.56, Temperature = 25 °C.

Where k_{obs} (min⁻¹) is the observed first-order reaction rate constant, which can be calculated from the slope of the line by plotting $\ln(O_3)/(O_3)_0$ vs the reaction time. As shown in Fig. S10, a good linearity was obtained in both the processes, which indicated that O₃ decomposition obeyed first order kinetics. The rate constants in the presence of NC-LaMnO₃ and NC-LaFeO₃ were 0.14 and 0.08 min⁻¹ which is 3.50 and 2.0 times higher than in single ozonation.

4.4. Evidence of surface reaction by FTIR

NC-LaMnO₃ as a high surface area catalyst, it is worthy to investigate its adsorption capability for organic intermediates produced during degradation of 2-CP and the role of surface reaction for TOC removal. So it can be hypothesized that most of the organic intermediates might be first absorb on NC-LaMnO₃ and then mineralized by ozone/reactive oxygen species. For this experiment, at first, single ozonation of 2-CP was conducted for 75 min, then the reaction medium was left for some time till the dissolved ozone was vanished. This solution was stirred with the catalysts for 75 min without ozone. It was shown that 15% and 5% of TOC was removed in the presence of NC-LaMnO₃ and CA-LaMnO₃ by adsorption respectively, suggesting that high surface area contributed to TOC removal (Fig. S11). To confirm the role of the surface reaction by ozone/reactive oxygen species in catalytic ozonation and adsorption, NC-LaMnO₃ was recycled from adsorption and catalytic ozonation experiments, dried, ultrasonicated in 1L deionized water for 75 min and TOC of solution was analyzed. It was found that the TOC of solution in case of adsorption (7.65 ppm) was higher than catalytic ozonation (0.52 ppm), which confirmed that adsorption of intermediates and their subsequent mineralization

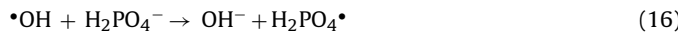
by ozone/reactive oxygen species contributed to TOC removal. To get further insights into the above mentioned surface reaction, the recycled NC-LaMnO₃ after adsorption of organic intermediates and catalytic ozonation was investigated by FTIR. As depicted in Fig. 3C, NC-LaMnO₃ after adsorption of organic intermediates indicated low intensity adsorption bands at about 1308, 1100 and 792 cm⁻¹ attributed to C—C, C—O and C—H stretching vibration of different organic intermediates [36]. However, NC-LaMnO₃ after ozonation of 2-CP did not show such adsorption bands and the spectra were nearly identical to those of the sample before ozonation. This phenomenon explains the positive role of high surface area perovskite to enhance the surface reaction by ozone/reactive oxygen species. This phenomenon also suggested that the adsorption of organic intermediates could not deactivate the catalyst due to the surface reaction by reactive oxygen species. Moreover, due to such process, ozone adsorption and its decomposition into reactive oxygen species on the catalyst surface could not be hindered.

4.5. Probing active sites and reactive oxygen species

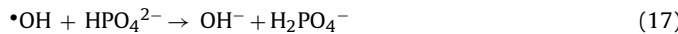
4.5.1. Use of phosphate and ATR-FTIR to probe surface hydroxyl groups as catalytic active sites

The concentration of surface hydroxyl groups of NC-LaMnO₃ was determined by TGA. The weight losses at approximately 120.90–300.26 and 300.26–600.85 °C could be attributed to weakly and strongly-bonded surface hydroxyl groups respectively (Fig. S4). The concentration of surface hydroxyl groups of NC-LaMnO₃ was calculated to be 2.70% (1.58 mmol g⁻¹). Phosphate is believed to be a stronger Lewis base than water, can substitute surface hydroxyl groups of the catalyst, which can hinder the interaction of O₃ with

the Lewis acid sites of the catalyst [37]. As shown in Fig. 3D, TOC removal was decreased in the presence of 90 mM phosphate in both ozonation and catalytic ozonation. However, the effect of phosphate to decrease TOC removal is obvious in catalytic process than in single ozonation. Furthermore, phosphate can also scavenge $\cdot\text{OH}$ as shown in the following Eqs.



$$k_2 < 105 \text{ M}^{-1} \text{ s}^{-1}$$



$$k_2 < 107 \text{ M}^{-1} \text{ s}^{-1}$$

The interaction of surface hydroxyl groups of the catalyst with phosphate was further investigated by ATR-FTIR. Instead of H_2O , D_2O was used to differentiate it from the bulk OH groups of NC-LaMnO₃. In the presence of phosphate, the intensity of absorption bands of MnO–D at 2478 and hydrogen bonded D₂O at 2386 and 1202 cm⁻¹ were significantly decreased while two new bands of phosphate vibrations appeared at 939 cm⁻¹ and 1082 cm⁻¹, suggesting that phosphate substituted the surface OH groups of NC-LaMnO₃ (Fig. 4A). Phosphate occupied the surface Lewis acid sites of NC-LaMnO₃ and lowered the chemisorptions of water, which subsequently inhibited the interaction with O₃ and catalytic activity [37].

As the data in Fig. S10 related to ozone decomposition showed a strong interaction of O₃ with NC-LaMnO₃ and NC-LaFeO₃ in aqueous solution. So such kind of interaction was also investigated by ATR-FTIR. It is a fact that more surface Lewis acid sites develop more surface hydroxyl groups and chemisorptions of water which ultimately increase the catalytic activity. Insitu ATR-FTIR experiments were conducted in the presence of D₂O to study the interaction of surface Lewis acid sites of the NC-LaMnO₃ and NC-LaFeO₃ and water molecules. The intensity of absorption bands of MnO–D at 2478 and hydrogen bonded D₂O at 2386 and 1202 cm⁻¹ for NC-LaMnO₃ are stronger than NC-LaFeO₃ suggesting that NC-LaMnO₃ have more surface Lewis acid sites owing to high adsorption of D₂O. These observations are in line with the TPD-NH₃ and TPD-CO₂ peaks intensities and catalytic activities. Moreover, the interaction of ozone with NC-LaMnO₃ and NC-LaFeO₃ in aqueous solution was investigated by insitu ATR-FTIR. After injecting ozone to NC-LaMnO₃ and NC-LaFeO₃ suspensions, the absorption bands at 2478, 2386 and 1202 cm⁻¹ are weak in NC-LaMnO₃ than in NC-LaFeO₃. This phenomenon reveals the strong interaction of ozone with NC-LaMnO₃ due to abundance of active sites [37,38].

4.5.2. Direct evidence of $\cdot\text{OH}$ production by fluorescence spectroscopy and EPR

$\cdot\text{OH}$ generation in catalytic ozonation was further investigated by applying 0.65 mM terephthalic acid as a fluorescence probe, which can react with $\cdot\text{OH}$ to produce a highly fluorescent 2-hydroxyterephthalic acid [39]. As shown in Fig. 4B at a wavelength of 425 nm, the fluorescence intensity gradually increased with time suggesting that $\cdot\text{OH}$ generation was increased in catalytic ozonation. As compared to ozonation alone, the fluorescence intensity was much higher in catalytic ozonation, which showed that the catalyst improved the production of $\cdot\text{OH}$ [37]. In order to further confirm the presence of $\cdot\text{OH}$ in the reaction system, the same fluorescence experiment was also carried out in the presence of TBA. It was found that the fluorescence intensity was significantly diminished in the presence of TBA in catalytic ozonation due to scavenging of $\cdot\text{OH}$. This proved a direct evidence for the involvement of $\cdot\text{OH}$ in the catalytic process.

EPR spectroscopy is more sensitive technique used to detect $\cdot\text{OH}$, superoxide ($\text{O}_2^{\bullet-}$) and singlet oxygen (${}^1\text{O}_2$) radicals. Spin-trapping reagent DMPO (5,5-dimethyl-1-pyrroline) is used in EPR experiments to detect $\cdot\text{OH}$ and $\cdot\text{O}_2^{\bullet-}$ while TEMP (2,2,6,6-tetramethyl-4-piperidone) is used to detect ${}^1\text{O}_2$ by measuring the spin-adducts DMPO– $\cdot\text{OH}$, DMPO– $\cdot\text{O}_2^{\bullet-}$ and TEMPO respectively. Radicals quenching experiments and fluorescence spectroscopy suggested that the $\cdot\text{OH}$ were the dominant reactive oxygen species in catalytic ozonation. To detect the generation of $\cdot\text{OH}$, catalytic ozonation was carried out in ultrapure water. The characteristics spectrum of the DMPO– $\cdot\text{OH}$ adducts (quartet lines with height ratio of 1:2:2:1) was observed, suggesting the generation of $\cdot\text{OH}$ (Fig. 4C). Moreover, instead of ultrapure water, methanol was used as a reaction medium to extend the half-life of $\text{O}_2^{\bullet-}$. However, no characteristics spectrum of the DMPO– $\cdot\text{O}_2^{\bullet-}$ was observed. Similarly for detecting ${}^1\text{O}_2$, no characteristic spectrum of the TEMPO adducts was observed. These all observations suggested that $\cdot\text{OH}$ rather than $\text{O}_2^{\bullet-}$ and ${}^1\text{O}_2$ radicals were the dominant reactive oxygen species.

4.5.3. Probing the generation of surface peroxide and surface atomic oxygen species by Raman spectroscopy

Some intermediate oxygen species such as surface atomic oxygen (O[−]) and surface peroxide (O₂^{2−}) can be formed on catalyst surface in water due to ozone decomposition. These species are also involved in catalytic ozonation. For this purpose, Raman spectroscopy is used to detect these species [28,40]. Before ozonation, two diagnostic Raman bands at about 500 and 598 cm⁻¹, attributed to bending and stretching Mn–O lattice vibration respectively were obtained (Fig. 4D) [41,42]. After ozonation for 20 min, the above mentioned peaks were shifted to 519 and 629 cm⁻¹. The quantum theory of Raman scattering suggested that a change of state is accomplished by the loss or gain of specific quanta of energy. The Raman shift can indicate the required energy for a bond to shift from ground state to the excited state. With ozonation, a little energy of ozone could activate Mn–O vibration, resulting in the Raman shift. [43,44]. These observations indicated that ozone is a powerful reactive oxidation agent. Moreover, the catalyst did not exhibit any peaks at approximately 828 and 938 cm⁻¹ after ozonation, which were usually assigned to O₂^{2−} and surface O[−] respectively [28,40,45]. These results indicated that ozone after adsorption on Lewis acid sites was not decomposed into surface peroxide and surface atomic oxygen species and these species were not involved in catalytic ozonation [45].

4.5.4. Investigating the role of electron transfer/redox couple (Mn⁺³/Mn⁺⁴) by XPS analysis and linear sweep voltammetry (LSV)

XPS was carried out to determine the chemical surface composition/state of NC-LaMnO₃ before and after ozonation. The % surface concentration of Mn/(La + Mn) is 38.31%. Fig. 5 shows the XPS spectra of Mn 2p and O 1s before and after ozonation. A peak at 642.0 eV is attributed to Mn 2p_{3/2}. Due to a little difference between the binding energies of Mn⁴⁺ and Mn³⁺, the main spectra can be divided into two peaks at binding energies of 641.88 and 643.30 eV, attributing to the coexistence of Mn³⁺ and Mn⁴⁺, respectively [46]. The relative content of the surface Mn⁴⁺ increased from 42.55 to 50.97%, while that of Mn³⁺ decreased from 57.45 to 49.03% after ozonation (Fig. 5A and B), suggesting that Mn³⁺ was oxidized to Mn⁴⁺ by ozone. It indicated that electrons were transferred from surface Mn³⁺, which might follow the sequence of Mn³⁺ → Mn⁴⁺ → Mn³⁺ redox reaction during the catalytic process. This phenomenon will be further explained in the following passages.

The O 1s spectra of the catalyst before and after ozonation exhibited peaks at the binding energies of 529.55 and 531.06 ascribed to surface lattice oxygen (O_L^{2−}) and surface adsorbed oxygen (O_A) or surface hydroxyl (OH) species respectively. O_L^{2−} and OH groups

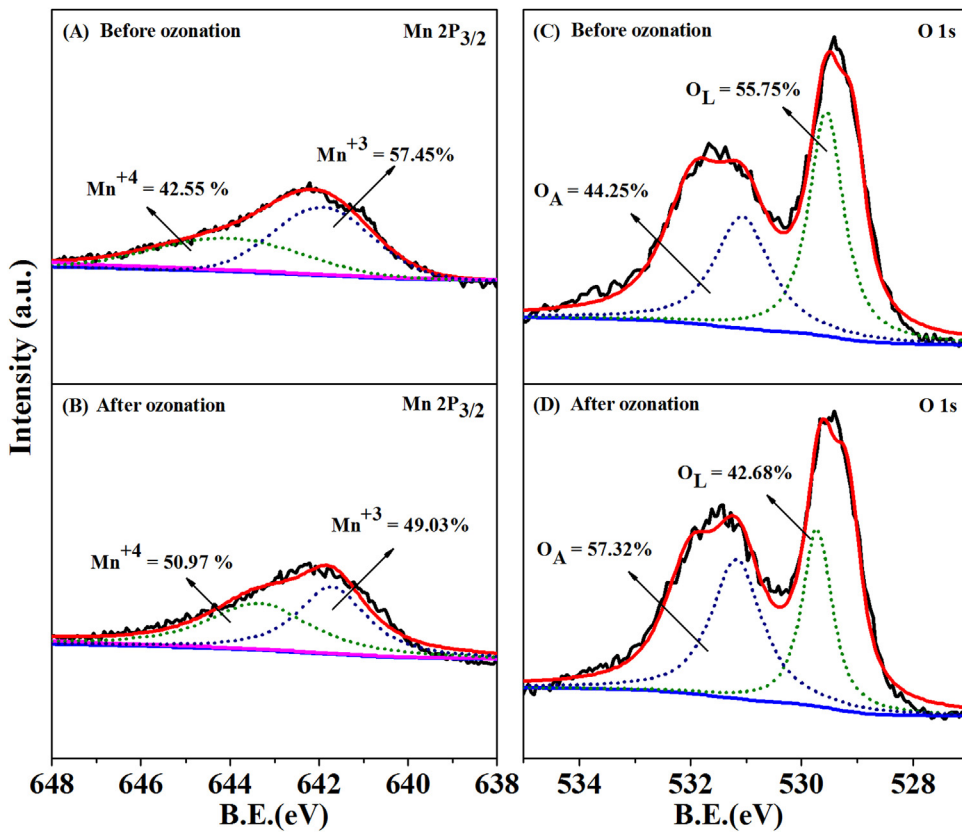


Fig. 5. Mn 2P_{3/2} and O 1s in XPS measurement before and after ozonation of NC-LaMnO₃.

play an important role in the oxidation reactions [45]. After ozonation, the relative contents of O_L reduced from 55.75 to 42.68%, while that of O_A increased from 44.25 to 57.32% (Fig. 5C and D). The increase in the adsorbed oxygen content might be due to the development of surface OH groups. The decrease in the lattice oxygen content indicated that its utilization took place, resulting in the reduction of Mn⁺⁴ to Mn⁺³. This decrease revealed that the lattice oxygen might be oxidized by Mn⁺⁴ releasing O₂ to the reaction system as shown in Eq. (33). These results showed that lattice oxygen and surface hydroxyl groups took part in the catalytic ozonation.

As shown by ATR-FTIR analysis, in the presence of O₃, the intensity of surface OH groups and chemisorbed water decreased, whereas XPS results indicated that the valence state of manganese and the amount of oxygen on the surface of changed. Thus, it

implied that the NC-LaMnO₃ surface provided the adsorption sites for O₃ and its activation, whereas manganese served as the active site for the transfer of electrons. At first, H₂O adsorbed and activated at the surface Lewis acid sites and then surface OH groups were formed. Simultaneously, O₃ was interconnected on the surface of the catalyst (MnOH₂⁺) via electrostatic attraction or hydrogen bonding, facilitating electron transfer (Fig. 7; step 2). In the next phase, H—O and O—O bonds were simultaneously weakened, due to which the intermediates were decomposed to HO₂[•], HO₃[•] and •OH on the catalyst surface (Fig. 7; step 3). This step is followed by a typical chain reaction on the surface of catalyst as well as in the liquid phase between ozone and HO₂[•] to produce •OH, which ultimately mineralize 2-CP (Fig. 7; step 4).

As it is already mentioned in the ATR-FTIR analysis, in the presence of ozone, the surface OH and chemisorbed water were decreased, so simultaneously the transfer of electrons took place from the surface Mn³⁺ to ozone. As a result of oxidation, the concentration of surface Mn⁴⁺ increased. To complete the redox reaction and maintain the electrostatic balance, the lattice oxygen would reduce Mn⁴⁺ to Mn³⁺ by electron transfer (Fig. 7 step 5). As a result, the oxygen vacancies occurred on the surface, which increased the oxygen surface adsorption ability of the catalyst. Then the oxygen-deficient bulk on the catalyst surface was replenished by ozone Eq. (34). To sum off it all, in the whole catalytic process, a cycling reaction in the sequence of Mn³⁺ → Mn⁴⁺ → Mn³⁺ was accomplished (Fig. 7; Step 6). During the course of oxidation, the transfer of electrons from the surface Mn³⁺ induced ozone decomposition to reactive oxygen species, while the lattice oxygen converted/reduced Mn⁴⁺ to Mn³⁺. So an electrostatic balance/redox couple between Mn³⁺/Mn⁴⁺ and O^{2−}/O₂ played a key role in catalytic activity.

As mentioned in XPS, the electron transfer progress is important for heterogeneous catalytic ozonation. Therefore, linear sweep

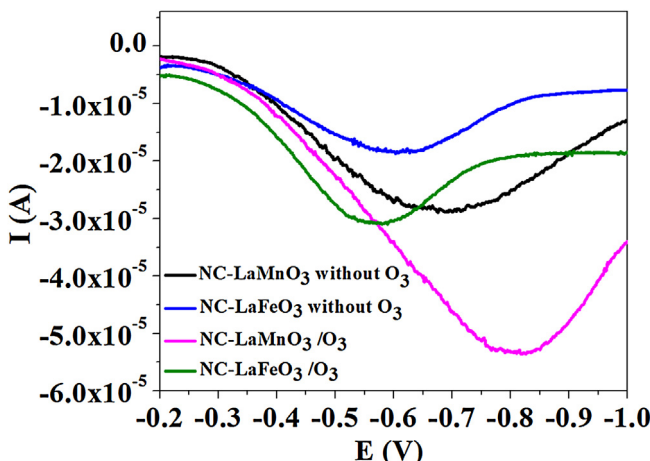


Fig. 6. LSV of NC-LaMnO₃ and NC-LaFeO₃ in the absence and presence of ozone.

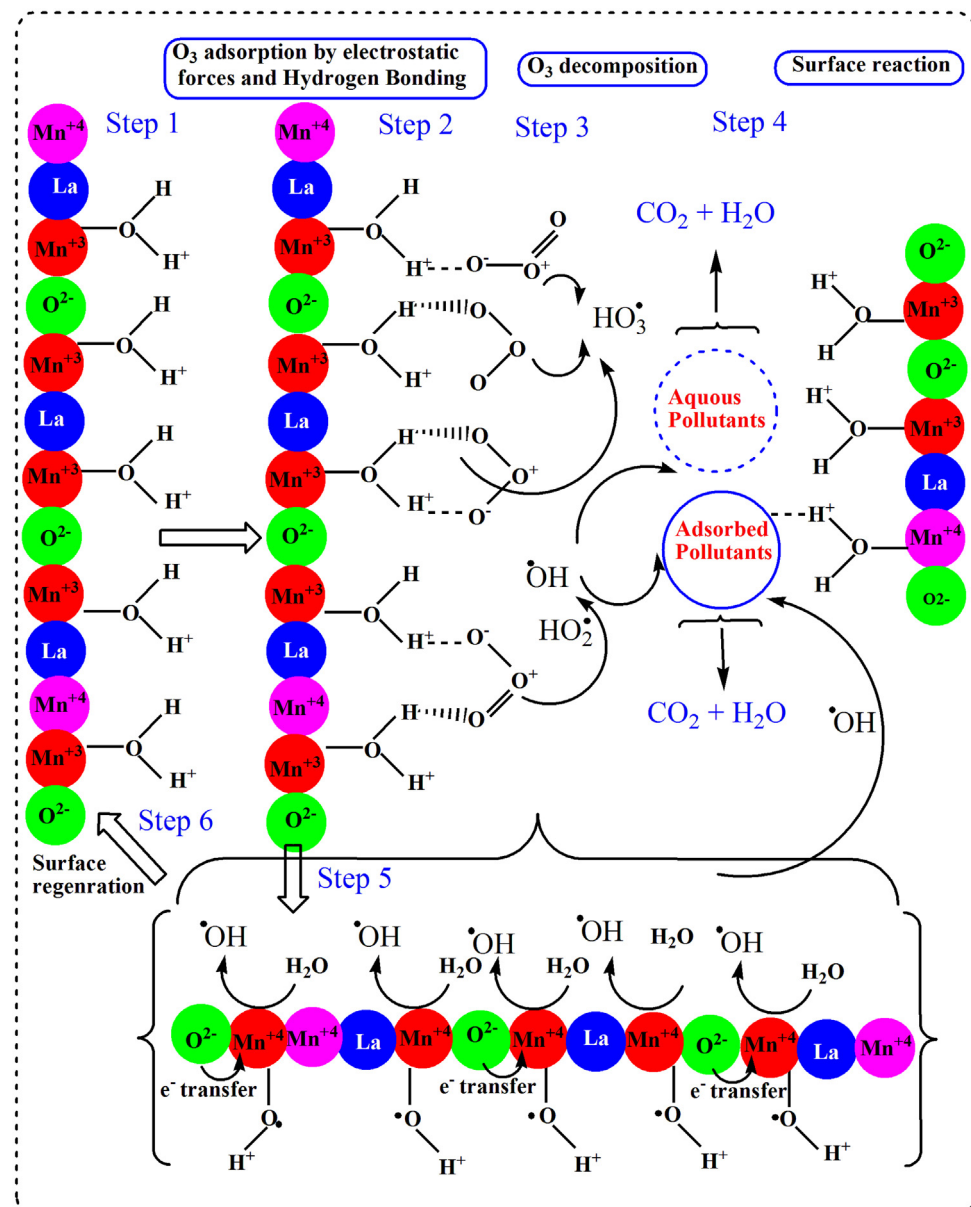


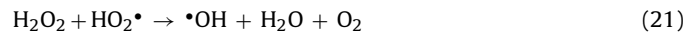
Fig. 7. Schematic representation of catalytic ozonation mechanism.

voltammetry (LSV) behavior of NC-LaMnO₃ and NC-LaFeO₃ was comparatively investigated in a 0.1 M Na₂SO₄ solution at water-catalyst interface in the presence and absence of ozone. An obvious and significantly high current signal in case of NC-LaMnO₃ was observed in the absence of ozone, verifying the presence of high surface charge on NC-LaMnO₃ than NC-LaFeO₃ (Fig. 6). However, in the presence of ozone, an enhancement in the reduction current intensity was observed, suggesting a possible reduction process occurred on the surface of catalysts with the decomposition of ozone. Similarly the reduction current in case of NC-LaMnO₃ was significantly increased as compared to NC-LaFeO₃. These observations indicated that a stronger interaction between the catalyst and O₃ as well as an interfacial electron transfer resulted in enhanced catalytic activity [47].

4.5.5. Detection of H₂O₂ production as oxidative intermediate species

H₂O₂ is also an important oxidant and the only stable active oxygen species used to produce •OH in advanced oxidation pro-

cesses. H₂O₂ is also produced in ozonation and catalytic ozonation from ozone decomposition [28]. H₂O₂ formation in ozonation alone and catalytic ozonation in the absence and presence of 2-CP was investigated. In the absence of 2-CP, the concentrations of H₂O₂ in catalytic ozonation was significantly higher than ozonation alone and increased continuously with increasing reaction time (Fig. S12). H₂O₂ was formed which initiated the production of •OH [32,34] as shown in the following Eqs. (18)–(21).



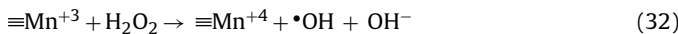
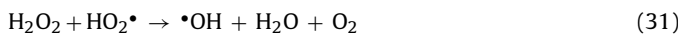
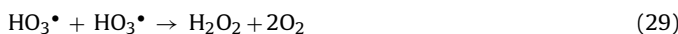
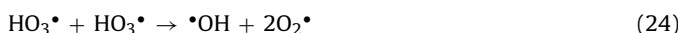
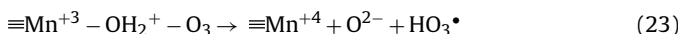
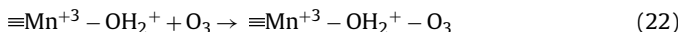
In the presence of 2-CP, the concentration of H₂O₂ was drastically reduced with time in ozonation alone and catalytic ozonation. This phenomenon might be due to the consumption of •OH during the mineralization of organic intermediates which suppressed the reaction 19. Moreover, H₂O₂ could also oxidize the surface Mn³⁺ to

Mn⁺⁴ and produce •OH, led to decrease the concentration of Mn⁺³ and increase Mn⁺⁴ [28] as shown in Eq. (32). So H₂O₂ played an important role in enhancement of catalytic activity.

4.6. Investigating the reducibility of the catalyst by TPR-H₂ measurements

H₂-TPR measurements were carried out to explore the reducibility of the catalyst before and after ozonation. Previous reports suggested that Mn²⁺ is the final oxidation state in the reduction process of manganese oxides but its complete reduction to metallic Mn⁰ does not occur for LaMnO₃ [48]. Furthermore, some fraction of Mn⁴⁺ could be present in NC-LaMnO₃, which creates crystal defects and over-stoichiometric oxygen. As shown in Fig. S13, before ozonation, the peak centered at approximately 582 °C is attributed to the reduction of Mn⁴⁺ to Mn³⁺ and the removal of the chemisorbed surface oxygen species while the peak at 826 °C is assigned to the reduction of Mn³⁺ to Mn²⁺ [48]. After ozonation, a broad shoulder at about 628 °C appeared, while the reduction peak at 582 °C was diminished into two smaller peaks at 418 and 515 °C (shifted to lower temperature), suggesting the reduction of Mn⁴⁺ into Mn³⁺.

To sum off it all, in light of our experimental observations in the above mentioned detailed discussion and reviews of the literature [28,32,34,45] the following mechanism in Eqs. (22)–(34) is proposed for the catalytic activity of NC-LaMnO₃. Moreover, the mechanism is summarized in schematic Fig. 7.



5. Conclusion

High surface area nanocast mesoporous perovskites with easily accessible active sites showed comparatively high catalytic activity in terms of TOC removal in ozonation of 2-chlorophenol than uncast counterpart perovskites as well as Mn₃O₄ and Fe₂O₃ prepared by conventional citric acid assisted route. TOC removal followed the order of NC-LaMnO₃ > NC-LaFeO₃ > CA-LaMnO₃ > CA-LaFeO₃ > Mn₃O₄ > Fe₃O₄. NC-LaMnO₃ showed good performance in terms of catalytic activity and stability. Neutral charged surface (MnOH) as well as protonated surface (MnOH₂⁺) was catalytically more active than deprotonated surface (MnO[−]) to decompose ozone into hydroxyl radicals. Organic and inorganic •OH quenchers and some advanced characterization techniques were used to discuss the mechanism of catalytic ozonation of selected NC-LaMnO₃ perovskite. •OH was found to be the dominant reactive oxygen species contributed to high catalytic activity.

Acknowledgements

This work was supported by National Natural Science Foundation of China (No. 21590813), Program for Changjiang Scholars and Innovative Research Team in University (IRT-13R05), and the Program of Introducing Talents of Discipline to Universities (B13012).

Appendix A. Supplementary data

Supplementary data associated with this article can be found, in the online version, at <http://dx.doi.org/10.1016/j.apcatb.2017.01.072>.

References

- [1] J. Chen, S. Tian, J. Lu, Y. Xiong, Appl. Catal. A: Gen. 506 (2015) 118–125.
- [2] H. Yan, W. Chen, G. Liao, X. Li, S. Ma, L. Li, Sep. Purif. Technol. 159 (2016) 1–6.
- [3] S. Afzal, X. Quan, S. Chen, J. Wang, D. Muhammad, J. Hazard. Mater. 318 (2016) 308–318.
- [4] Y. Wang, Y. Xie, H. Sun, J. Xiao, H. Cao, S. Wang, ACS Appl. Mater. Interfaces 8 (2016) 9710–9720.
- [5] N.A. Merino, B.P. Barbero, P. Grange, L.E. Cadús, J. Catal. 231 (2005) 232–244.
- [6] D.B. Meadowcroft, Nature 226 (1970) 847–848.
- [7] W.B. Li, J.X. Wang, H. Gong, Catal. Today 148 (2009) 81–87.
- [8] G. Biasque, Y. Schuurman, J. Catal. 276 (2010) 306–313.
- [9] B.P. Barbero, J.A. Gamboa, L.E. Cadús, Appl. Catal. B: Environ. 65 (2006) 21–30.
- [10] G. Sinquin, C. Petit, J.P. Hindermann, A. Kiennemann, Catal. Today 70 (2001) 183–196.
- [11] A.E. Giannakas, T.C. Vaimakis, A.K. Ladavos, P.N. Trikalitis, P.J. Pomonis, J. Colloid Interface Sci. 259 (2003) 244–253.
- [12] G. Groppi, M. Bellotto, C. Cristiani, P. Forzatti, P.L. Villa, Appl. Catal. A: Gen. 104 (1993) 101–108.
- [13] A. González, E. Martínez Tamayo, A. Beltrán Porter, V. Cortés Corberán, Catal. Today 33 (1997) 361–369.
- [14] R. Leanza, I. Rossetti, L. Fabbrini, C. Oliva, L. Forni, Appl. Catal. B: Environ. 28 (2000) 55–64.
- [15] A. Giroir-Fendler, M. Alves-Fortunato, M. Richard, C. Wang, J.A. Díaz, S. Gil, C. Zhang, F. Can, N. Bion, Y. Guo, Appl. Catal. B: Environ. 180 (2016) 29–37.
- [16] R.K.C. de Lima, M.S. Batista, M. Wallau, E.A. Sanches, Y.P. Mascarenhas, E.A. Urquieta-González, Appl. Catal. B: Environ. 90 (2009) 441–450.
- [17] Z. Sarshar, F. Kleitz, S. Kaliaguine, Energy Environ. Sci. 4 (2011) 4258–4269.
- [18] G. Martinelli, M.C. Carotta, M. Ferroni, Y. Sadaoka, E. Traversa, Sens. Actuators B: Chem. 55 (1999) 99–110.
- [19] F.J. Rivas, M. Carbajo, F.J. Beltrán, B. Acedo, O. Gimeno, Appl. Catal. B: Environ. 62 (2006) 93–103.
- [20] M. Carbajo, F.J. Beltrán, F. Medina, O. Gimeno, F.J. Rivas, Appl. Catal. B: Environ. 67 (2006) 177–186.
- [21] M. Carbajo, F.J. Beltrán, O. Gimeno, B. Acedo, F.J. Rivas, Appl. Catal. B: Environ. 74 (2007) 203–210.
- [22] C.A. Orge, J.J.M. Órfão, M.F.R. Pereira, B.P. Barbero, L.E. Cadús, Appl. Catal. B: Environ. 140–141 (2013) 426–432.
- [23] S.M. Hao, J. Qu, Z.S. Zhu, X.Y. Zhang, Q.Q. Wang, Z.Z. Yu, Adv. Funct. Mater. 26 (2016) 7334–7342.
- [24] L. Lyu, L. Zhang, C. Hu, M. Yang, J. Mater. Chem. A 4 (2016) 8610–8619.
- [25] R.A. Doong, R.A. Maithreepala, S.M. Chang, Water Sci. Technol. 42 (2000) 253–260.
- [26] M.M. Nair, S. Kaliaguine, F. Kleitz, ACS Catal. 4 (2014) 3837–3846.
- [27] A.G. Bhavani, W.Y. Kim, J.S. Lee, ACS Catal. 3 (2013) 1537–1544.
- [28] J. Bing, C. Hu, Y. Nie, M. Yang, J. Qu, Environ. Sci. Technol. 49 (2015) 1690–1697.
- [29] Z. Wu, A.K.P. Mann, M. Li, S.H. Overbury, J. Phys. Chem. C 119 (2015) 7340–7350.
- [30] J. Ma, N.J.D. Graham, Water Res. 34 (2000) 3822–3828.
- [31] Y. Yang, J. Ma, Q. Qin, X. Zhai, J. Mol. Catal. A: Chem. 267 (2007) 41–48.
- [32] L. Zhao, Z. Sun, J. Ma, H. Liu, J. Mol. Catal. A: Chem. 322 (2010) 26–32.
- [33] L. Hao, D. Huiping, S. Jun, J. Mol. Catal. A: Chem. 363–364 (2012) 101–107.
- [34] L. Zhao, J. Ma, Z. Sun, H. Liu, Appl. Catal. B: Environ. 89 (2009) 326–334.
- [35] M.S. Elowitz, U. von Gunten, Ozone 21 (1999) 239–260.
- [36] S.J. Hug, D. Bahnemann, J. Electron Spectrosc. Relat. Phenom. 150 (2006) 208–219.
- [37] H. Zhao, Y. Dong, P. Jiang, G. Wang, J. Zhang, K. Li, Catal. Sci. Technol. 4 (2014) 494–501.
- [38] W. Li, Z. Qiang, T. Zhang, F. Cao, Appl. Catal. B: Environ. 113–114 (2012) 290–295.
- [39] K.-i. Ishibashi, A. Fujishima, T. Watanabe, K. Hashimoto, J. Photochem. Photobiol. A: Chem. 134 (2000) 139–142.
- [40] T. Zhang, W. Li, J.P. Croué, Environ. Sci. Technol. 45 (2011) 9339–9346.
- [41] T. Gao, M. Glerup, F. Krumeich, R. Nesper, H. Fjellvåg, P. Norby, J. Phys. Chem. C 112 (2008) 13134–13140.
- [42] C.M. Julien, M. Massot, C. Poinsignon, Spectrochim. Acta Part A Mol. Biomol. Spectrosc. 60 (2004) 689–700.

- [43] G. Gouadec, P. Colombe, *Prog. Cryst. Growth Charact. Mater.* 53 (2007) 1–56.
- [44] Y. Dong, K. Li, P. Jiang, G. Wang, H. Miao, J. Zhang, C. Zhang, *RSC Adv.* 4 (2014) 39167–39173.
- [45] H. Zhao, Y. Dong, P. Jiang, G. Wang, J. Zhang, K. Li, C. Feng, *New J. Chem.* 38 (2014) 1743–1750.
- [46] S. Ponce, M.A. Peña, J.L.G. Fierro, *Appl. Catal. B: Environ.* 24 (2000) 193–205.
- [47] F. Nawaz, Y. Xie, J. Xiao, H. Cao, Z.A. Ghazi, Z. Guo, Y. Chen, *Catal. Sci. Technol.* 6 (2016) 7875–7884.
- [48] C. Zhang, C. Wang, W. Hua, Y. Guo, G. Lu, S. Gil, A. Giroir-Fendler, *Appl. Catal. B: Environ.* 186 (2016) 173–183.